Line-shape study of two-color–three-photon ionization of Rb atoms

Ivo Cacelli,[1] Andrea Fioretti,[2,3] Carlo Gabbanini,[2] Marina Mazzoni,[4,5] and Maurizio Persico[1]
[1]*Dipartimento di Chimica e Chimica Industriale, Università di Pisa, Via Risorgimento 35, I-56126 Pisa, Italy*
[2]*Istituto per i Processi Chimico-Fisici del CNR, Via G. Moruzzi 1, I-56124 Pisa, Italy*
[3]*Unità INFM, Dipartimento di Fisica, Università di Pisa, Piazza Torricelli 2, I-56127 Pisa, Italy*
[4]*Istituto di Elettronica Quantistica del CNR, Via Panciatichi 56, I-50127 Firenze, Italy*
[5]*Unità INFM, Sez. A, Dipartimento di Fisica, Università di Firenze, Largo E. Fermi 2, 50125 Firenze, Italy*
(Received 20 February 2002; revised manuscript received 15 May 2002; published 21 August 2002)

We report on the analysis of the line shapes in a two-color, three-photon ionization process of rubidium atoms in a magneto-optical trap. A cw and a pulsed laser are tuned almost at resonance with the $5^2S_{1/2}$-$5^2P_{3/2}$ and the $5^2P_{3/2}$-$6^2D_{5/2}$ transitions, respectively. The line shapes, recorded as functions of the pulsed laser wavelength, are strongly asymmetric with respect to the near resonance peak positions: in fact, they present long tails only on one side, according to the sign of the detuning of the cw laser. Moreover, the signal is overall stronger for negative than for positive detunings. Theoretical considerations based on the Autler-Townes scheme and computer simulations of the excitation-ionization dynamics show that the main source of asymmetry is the coupling of the two ionization pathways going through the $6^2D_{3/2}$ and $6^2D_{5/2}$ levels. In order to reproduce the experimental line shapes one must take into account the variability of the pulsed laser intensity and its finite coherence time.

DOI: 10.1103/PhysRevA.66.023408 PACS number(s): 32.80.Rm

I. INTRODUCTION

The analysis of spectral line shapes in a vapor gives information on the physical processes that perturb atoms or molecules. In the last decades a large effort has been devoted to the interpretation of line shapes modified by collisions and/or laser fields [1]. Here we report on a study of photoionization line shapes obtained when a pulsed laser field perturbs the near resonant atomic levels involved in a two-color ($5^2S_{1/2}$-$5^2P_{3/2}$ plus $5^2P_{3/2}$-$6D_J$), three-photon ionization process. Anomalous line shapes have been observed in the ion spectra during an experiment aimed at producing and detecting translationally cold molecules [2] in a rubidium magneto-optical trap (MOT). A cw laser tuned to the red side of the atomic resonance photoassociates the trapped atoms by creating quasi-molecules in the excited state that may have a nonzero probability to decay into ground-state molecules. The possible presence of translationally cold molecules is detected by time-of-flight spectroscopy after photoionization by a pulsed laser. When the photoassociation laser is detuned 3–10 GHz from the $5S_{1/2}$-$5P_{3/2}$ atomic resonance, that corresponds to about 1000 natural linewidths (the Doppler width is negligible at the temperature of the trapped atoms), we should expect the population of excited state atoms to be very low. However, when a pulsed laser is scanned on a transition that connects the $5P_{3/2}$ level to a highly excited level through a dipole-allowed transition, we observe a huge increase in the number of produced atomic ions and the resulting line shape is strongly asymmetric. This effect is not peculiar of cold atoms but it happens also in a thermal vapor, as we verified. However, the utilization of a MOT gives some advantages related to better defined conditions of light-atom interactions.

The particular laser combination we used, made of cw and pulsed sources, is employed when photoassociation spectroscopy together with a very sensitive detection is required. Such two-color excitation is similar to that recently used by Duncan *et al.* for the $5D_{5/2}$ ionization cross-section determination using trapped atoms [3]. As the present study is based on the photoionization signal from the high-lying $6D_J$ levels, we also had the possibility to evaluate the experimental ionization probability and to perform a comparison with a photoionization cross section computed for a simulation of the entire line shape. Concerning the line shape, the main physical process is the well-known dynamical Stark shift. When scanning the pulsed laser on the P-D transition, we must consider that the dynamical Stark effect influences both excitation pathways, $5^2S_{1/2}$-$5^2P_{3/2}$-$6^2D_{5/2}$ and $5^2S_{1/2}$-$5^2P_{3/2}$-$6^2D_{3/2}$, with cooperative and competing effects. An evaluation of the ionization line shape excluding these effects is performed with a simplified model which separates the contributions of the two levels, while they are taken into account a second time with a simulation including all the levels at once.

Photoionization line-shape simulation with the simultaneous presence of cw and pulsed lasers has never been faced before, since only pulsed lasers are normally used in multiphoton ionization. Much attention was devoted in the past to study the influence of the coherent properties of these laser sources, especially the finite bandwidth and fluctuations for their implication in both resonant and off-resonant interactions with atom levels [4–10]. For example, in an experiment of doubly resonant three photon ionization [9,10], the nonmonochromaticity of the strong pulsed laser inducing the ac Stark splitting of the intermediate level reversed the normal (as produced by perfectly monochromatic fields) peak intensities of the ionization probabilities. In our case, since we worked in different laser conditions, the intermediate level was shifted and not significantly split. Therefore we found other forms of asymmetry, in particular concerning the nonequivalence of positive and negative detunings of the cw laser. We found that phase fluctuations are important for the

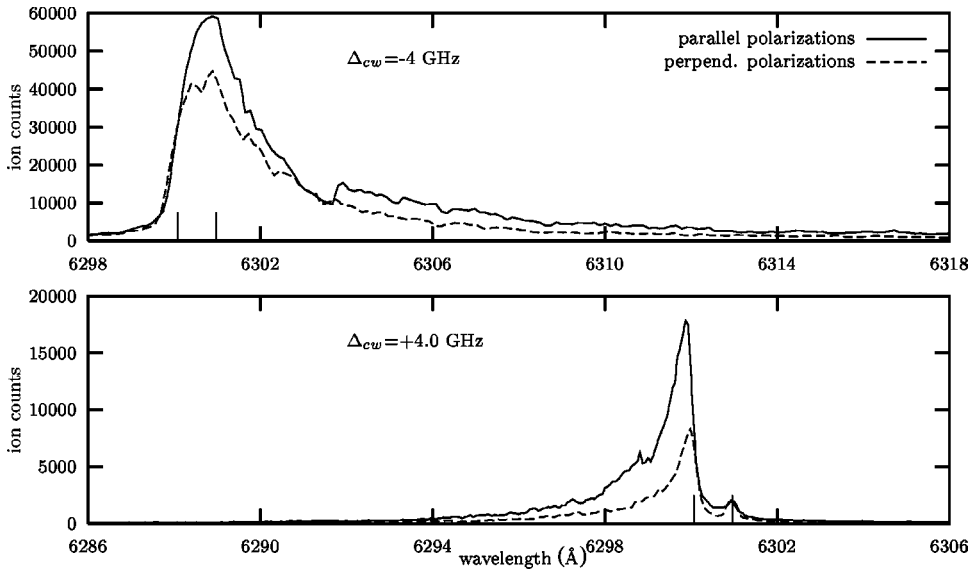

FIG. 1. Experimental line shapes, i.e., ion counts as functions of the pulsed laser wavelength. Peak intensity of 40 MW/cm^2. Full lines: parallel polarizations of the cw and pulsed lasers. Dashed lines: perpendicular polarizations. Vertical bars mark the $5^2P_{3/2}\rightarrow 6^2D_{3/2}$ and $5^2P_{3/2}\rightarrow 6^2D_{5/2}$ transitions, at $\lambda = 6300.96$ and 6300.07 Å, respectively.

ionization line shapes close to the two $5^2P_{3/2}$-6^2D_J unperturbed transition frequencies. In order to reproduce the experimental line shapes it was also important to consider the spatial inhomogeneities of the pulsed laser beam and the dispersion of pulse intensities.

The paper is organized as follows: in the next section the experimental setup and the main characteristics of the observed line shapes are presented; in the following section the theoretical analysis is presented, divided into a subsection concerning the photoionization cross section (Sec. III A), one where a simplified treatment of the line shape is performed (Sec. III B), and another where the line shapes are simulated (Sec. III C). Finally the last section compares the theoretical and experimental line shapes.

II. EXPERIMENT

The apparatus is composed of a vapor cell, the lasers to create the MOT, the lasers to induce excitation and ionization of the trapped atoms, and the detection system. The cell is a stainless-steel sphere having several flanges with windows to allow for optical access and one for a channeltron multiplier. It is connected to an ion pump that keeps the vacuum below 10^{-8} Torr. A valve separates the cell from a rubidium reservoir and permits the regulation of the background Rb pressure inside the cell. The MOT is created by a magnetic field gradient, produced by two coils in anti-Helmholtz configuration, and by three laser beam pairs of nearly 1 cm diameter, propagating in orthogonal directions and retroreflected; the laser polarizations are chosen to make a standard σ^+/σ^- MOT. The trapping laser is a 50 mW cw diode laser injected by an extended cavity diode laser having a linewidth below 1 MHz; it is frequency locked about 10 MHz to the red side of the $F=3\rightarrow F'=4\mathrm{D}_2$ transition of ^{85}Rb at 780 nm. On two of the three axis another diode laser, tuned to the $F=2\rightarrow F'=3\mathrm{D}_2$ resonance, is superposed; it avoids optical pumping on the lower hyperfine level of the ground state. The MOT, that is monitored by a charge coupled device camera, has a maximum density of a few 10^{10} atoms/cm^3 and a volume of a fraction of mm^3, with an atomic temperature near the Doppler limit (141 μK). Excitation of cold atoms at any detuning near the $5P_{3/2}$ level is provided by a distributed Bragg reflector (DBR) diode laser (Yokogawa YL78XNW) of 5 mW output power and 1 MHz linewidth. It is directed at 45° with respect to the *x* and *y* axis of the MOT and is focused to have a power density of about 1 W/cm^2 at the trap position. In some measurements a more powerful diode laser has replaced the DBR diode laser. The polarization of the diode laser can be rotated by using a $\lambda/2$ plate.

The photoionization of cold atoms is provided by a pulsed dye laser, which is sent counterpropagating to the DBR laser (we have seen that a different geometry with copropagating beams does not influence the results). The pulsed dye laser is pumped by the second harmonic of a Nd:YAG laser and operates with DCM dye. The typical output energy is about 1 mJ in a pulse of 3 ns at 10 Hz repetition rate; this laser beam is focused on the MOT resulting in a maximum power density of the order of 50 MW/cm^2. The waist of the pulsed dye laser has been accurately measured by using a razor blade and a micrometer translator. An acousto-optic modulator positioned on the trapping laser path enables one to shut off this laser when required. The ions generated after the dye laser pulses are detected by a channeltron multiplier. The signal, after amplification, is sent to a boxcar integrator triggered by the laser pulse. The gate of the boxcar is delayed by the time-of-flight of the atomic ions produced from the MOT, i.e., 1.8 μs.

The experiment runs as follows. The MOT is loaded with nearly 10^7 atoms and at a given time the MOT lasers are switched off leaving the cold atoms under the exciting action of only the cw DBR diode laser, tuned at a given detuning near the $5P_{3/2}$ level. After a few microseconds, i.e., when a ''stationary'' regime is reached, the pulsed laser is shot, and the ion signal is subsequently recorded. This sequence is repeated at 10 Hz rate while varying either the cw or the pulsed laser wavelength. Signals are averaged over 30 laser shots.

Typical observed line shapes as a function of the pulsed

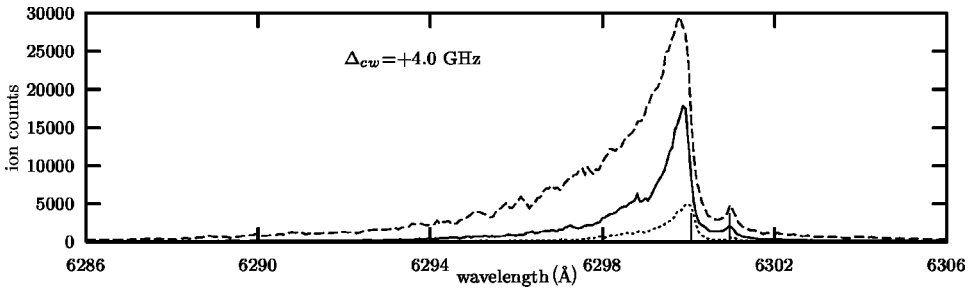

FIG. 2. Experimental line shapes with different peak intensities of the pulsed laser. The polarizations of the cw and pulsed lasers are parallel. Vertical bars mark the $5^2P_{3/2}\rightarrow 6^2D_{3/2}$ and $5^2P_{3/2}\rightarrow 6^2D_{5/2}$ transitions at $\lambda = 6300.96$ and 6300.07 Å, respectively.

laser wavelength are shown in Fig. 1 for two detunings Δ_{cw} of the cw laser. The line shape is strongly asymmetric with a long tail towards the blue for a positive detuning of the diode laser and with an even longer red tail when the detuning is reversed. In both cases the maximum is found in the proximity of the $5^2P_{3/2}$-$6^2D_{5/2}$ resonance, but for positive Δ_{cw} the peak is sharper and is accompanied by a weaker resonance at about 6301 Å, clearly due to the $5^2P_{3/2}$-$6^2D_{3/2}$ transition. For negative Δ_{cw} the maximum is taller and broader, so that it overlaps the $5^2P_{3/2}$-$6^2D_{3/2}$ resonance. In fact, for slightly different conditions, we obtained a forked peak [11], which is also found in the case of perpendicular polarizations of the cw and pulsed lasers. The dependence of the line shapes on the pulsed laser intensity is shown in Fig. 2. In this case, it is evident that the increase of the pulsed laser intensity causes not only a higher ion peak intensity but also longer tails.

III. THEORETICAL LINE SHAPES

In this section we present computer simulations of the line shape of the photoionization signal as a function of the pulsed laser wavelength. The standard simulation will take into account four bound levels ($5^2S_{1/2}$, $5^2P_{3/2}$, $6^2D_{3/2}$, and $6^2D_{5/2}$) and the continuum states of ^2P and ^2F symmetry, coupled by dipole interactions with a cw field and a coherent laser pulse. We also developed a simplified theoretical model in which the two sublevels $6^2D_{3/2}$ and $6^2D_{5/2}$ are considered separately in two different ionization routes. In particular, we proceeded from the simplest theoretical model, i.e., a Floquet treatment of the three state systems $5^2S_{1/2}$-$5^2P_{3/2}$-$6^2D_{3/2}$ and $5^2S_{1/2}$-$5^2P_{3/2}$-$6^2D_{5/2}$, to simulations of the full process, including the ionization step (see Fig. 3). The simpler treatment reproduces the main features of the experimental spectra and the results as reported in Sec III B.

In most of the calculations we shall assume the following form for the radiation electric field:

$$\mathcal{E}(t)=\mathcal{E}_{\rm cw}^{(0)}\cos(\Omega_{\rm cw}t)+\mathcal{E}_{\rm pul}^{(0)}f(t-t_0)\cos(\Omega_{\rm put}t), \qquad (1)$$

where the pulse envelope has the form:

$$f(t-t_0)=\cos\left(\frac{\pi(t-t_0)}{2\tau}\right) \qquad (2)$$

for $|t-t_0|\leq\tau$ and vanishes for $|t-t_0|>\tau$. The intensity of the cw laser is $I_{\rm cw}=\mathcal{E}_{\rm cw}^{(0)^2}\varepsilon_0 c/2$ and the peak intensity of the pulsed laser is $I_{\rm pul}=\mathcal{E}_{\rm pul}^{(0)^2}\varepsilon_0 c/2$. This finite basis pulse envelope was chosen because of its computational advantages. However, we also tested the effect of a Gaussian pulse envelope, which should reproduce more precisely the experimental conditions (see Sec. IV). We shall call $\Delta_{\rm cw}$ the detuning of the cw radiation of frequency $\Omega_{\rm cw}$ with respect to the $5^2S_{1/2}$-$5^2P_{3/2}$ transition ($\omega_1=12\,816.56\ {\rm cm}^{-1}$): $\Delta_{\rm cw}=\Omega_{\rm cw}-\omega_1$; in the same way, $\Delta_{\rm pul}$ is the detuning of the pulsed laser with respect to the $5^2P_{3/2}$-$6^2D_{5/2}$ transition ($\omega_2=15\,872.85\ {\rm cm}^{-1}$): $\Delta_{\rm pul}=\Omega_{\rm pul}-\omega_2$.

As shown in the preceding section and illustrated in more detail later on, the line shapes depend on the detuning $\Delta_{\rm cw}$ of the cw laser with respect to the $5^2S_{1/2}$-$5^2P_{3/2}$ transition, on the peak intensity and duration of the pulse, and on other characteristics of the two laser beams. As a complete explo-

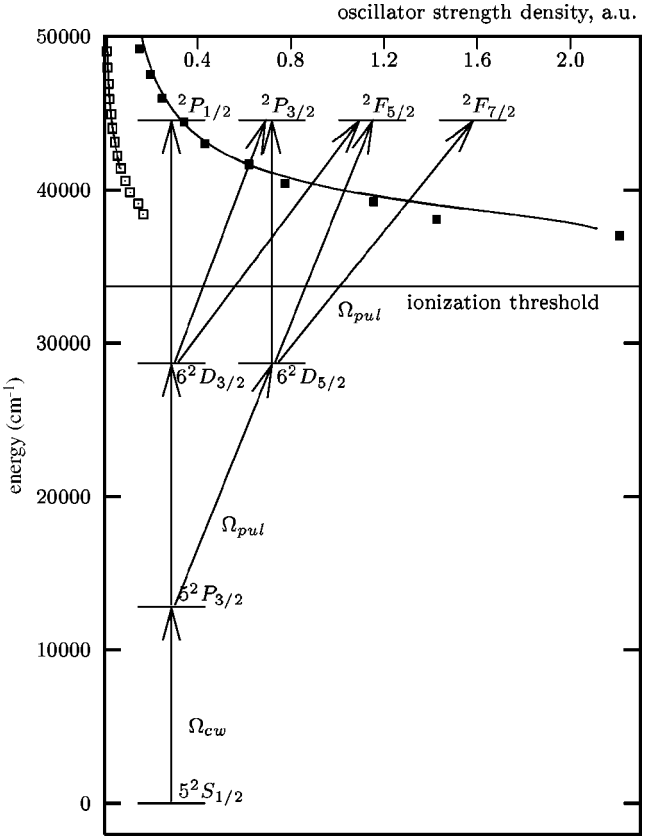

FIG. 3. Relevant atomic levels and dipole allowed transitions. In the upper panel we show the *ab initio* oscillator strength density, as a function of the continuum state energy, for the ionizing transitions $6^2D_J\rightarrow{}^2P_{J'}$ (open squares) and $6^2D_J\rightarrow{}^2F_{J'}$ (closed squares). The lines represent the analytic fit of the oscillator strength used in the simulations (see Sec. III B).

ration of all combinations of laser parameters is not practical, we have performed a limited study of the influence of the most important variables. In most cases, the values we have chosen are representative of the experimental conditions.

The intensity of the cw laser has been fixed at $I_{cw}=1\ \mathrm{W/cm^2}$: we have verified that the photoionization signal is simply proportional to I_{cw}. Two detunings are systematically investigated: $\Delta_{cw}=\pm 0.12\ \mathrm{cm^{-1}}=\pm 3.6\ \mathrm{GHz}$. The peak intensity and pulse duration of the pulsed laser are $I_{pul}=40\ \mathrm{MW/cm^2}$ and $\tau=3$ ns, unless stated otherwise. In most cases, the polarizations of the two lasers are assumed to be parallel, but perpendicular polarizations have also been tried.

Equations (1) and (2) represent the electric fields produced by perfectly coherent sources. We know, from a measurement of the pulsed laser linewidth (about 10 GHz), that its coherence time is much shorter than the pulse length (3 ns). For most simulations, we have taken into account the linewidth of the pulsed laser *a posteriori*, by convolution of the computed line shapes with a Gaussian function of FWHM=10 GHz (or 0.33 $\mathrm{cm^{-1}}$). This procedure is in principle not completely correct because of the nonlinearity of the Autler-Townes effect, but, as a matter of fact, the convolution has a negligible effect on all features of the spectra, with the exception of the narrowest peaks, associated with the $5^2P_{3/2}$-$6^2D_{3/2}$ transition. Such peaks would be very tall and sharp without convolution, a clearly unphysical feature not present in the experimental spectra. The finite coherence time of the laser has been taken into account explicitly in a set of simulations, which show the same smoothing effect as the simpler convolution procedure (see Sec. IV). Other features of the line shape are influenced by the finite coherence time, in a way that improves the agreement between measurements and simulations; however, since the changes are not dramatic, one can confidently use the simulations based on Eqs. (1) and (2) to investigate the dependence of the process on other laser parameters.

A. Photoionization cross sections

The evaluation of the relevant discrete-discrete and discrete-continuum dipole transition moments requires the knowledge of the ground and excited electronic states of the system. In the single particle frozen core approximation these states are written as $|\Phi^{N-1}\varphi_{\epsilon lm}\rangle$ where $|\Phi^{N-1}\rangle$ is the closed shell single determinant with $N-1$ electrons, obtained by removing the $5s$ spin orbital from the HF ground-state configuration of the Rb atom. ϵ is the discrete or continuum energy index, *l,m* represent the usual spherical harmonics indexes and the antisymmetrization is implicitly included. In this approximation the excited spin orbitals $|\varphi_{\epsilon lm}\rangle$'s are determined by solving the following static exchange equation

$$[T+V_{ne}+G^{N-1}]|\varphi_{\epsilon lm}\rangle=\epsilon|\varphi_{\epsilon lm}\rangle, \tag{3}$$

where T is the kinetic energy operator, V_{ne} is the nuclear attraction potential, and the operator G includes the Coulombic and exchange terms arising from the orbitals included in the $|\Phi^{N-1}\rangle$ state. To obtain a reliable description of the orbitals lying both in the discrete and the continuum energy range, they are projected onto large basis sets of Slater-type orbitals (STO) and STO* cos(*kr*) functions [12]. The latter have been proved to represent with high accuracy the typical oscillations of the continuum orbitals up to large values of the radial coordinate. This allows us to recover the proper normalization to unit energy range for the continuum orbitals.

These calculations provide spinless matrix elements for the d_z component of the dipole moment, which are then transformed to the relevant angular momentum eigenstate basis by the appropriate Clebsch-Gordan coefficients. We obtain $\langle 5s|d_z|5p\rangle=3.425$ a.u. and $\langle 5p|d_z|6d\rangle=0.446$ a.u. The former matrix element corresponds to an oscillator strength $f(5s-5p)=0.90$, to be compared with the experimental value of 1.00 [13,14] and with previous calculations which yielded $f(5s-5p)=0.95$–1.06 [15,16]. The oscillator strength densities $f=\frac{2}{3}(\epsilon-\epsilon_{6d})\langle 6d|d_z|\epsilon\rangle^2$ of the ionizing transitions starting from the $6d$ orbital are reported in Fig. 3 as functions of the final p or f orbital energy ϵ. At $\lambda=6300$ Å, the cross sections are 0.12 Mb for the d-p transition and 1.32 Mb for the d-f one.

B. Simplified treatment of the line shape

The simplified theory of ionization assumes that the ionization rate is the product of two factors: the time-averaged population of the 6^2D levels and the probability of one-photon ionization starting from the same levels, which is a linear function of the pulsed laser intensity. This ansatz will be confirmed later on by explicit simulations. We shall treat now the $6^2D_{3/2}$ and $6^2D_{5/2}$ levels independently, so that two separate three-state systems will be considered: $5^2S_{1/2}$-$5^2P_{3/2}$-$6^2D_{3/2}$ and $5^2S_{1/2}$-$5^2P_{3/2}$-$6^2D_{5/2}$. With these assumptions, and with laser intensities $I_{cw}\approx 1\ \mathrm{W/cm^2}$ and $I_{pul}\approx 10$–$100\ \mathrm{MW/cm^2}$, respectively, the $5^2S_{1/2}$-$5^2P_{3/2}$-$6^2D_{5/2}$ system is in the condition to exhibit a typical Autler-Townes effect [17].

A straightforward Floquet treatment, based on the dressed levels $5^2S_{1/2}+\hbar\Omega_{pul}$, $5^2P_{3/2}$ and $6^2D_{5/2}-\hbar\Omega_{pul}$, would yield a resonance for

$$\overline{\Delta_{pul}}=A\frac{1}{\Delta_{cw}}\left(1+B\frac{I}{\Delta_{cw}}\right)^{-1}, \tag{4}$$

where I is the intensity of the strong laser, $A=2\pi\langle 5^2P_{3/2}|d_z|6^2D_{5/2}\rangle^2/c=6.15\times 10^{-8}$ and $B=2\pi\langle 5^2S_{1/2}|d_z|5^2P_{3/2}\rangle^2/c=8.8\times 10^{-10}$ (in units such that detunings are in $\mathrm{cm^{-1}}$ and intensities in $\mathrm{W/cm^2}$). As far as the term BI/Δ_{cw} is a small correction, the detuning $\overline{\Delta_{pul}}$ at which the resonance is centered would be approximately proportional to I/Δ_{cw}, with the same sign as Δ_{cw}. The line shape, as a function of Δ_{pul}, would be approximately Lorentzian, taller and narrower for $\Delta_{cw}>0$ than for $\Delta_{cw}<0$. This asymmetry with respect to a change in sign of Δ_{cw}, represented by the BI/Δ_{cw} term in Eq. (4), is due to the off-resonant coupling of the $5^2S_{1/2}$ and $5^2P_{3/2}$ states through the pulsed laser (see Fig. 4), which shifts the $5^2P_{3/2}$ level upwards.

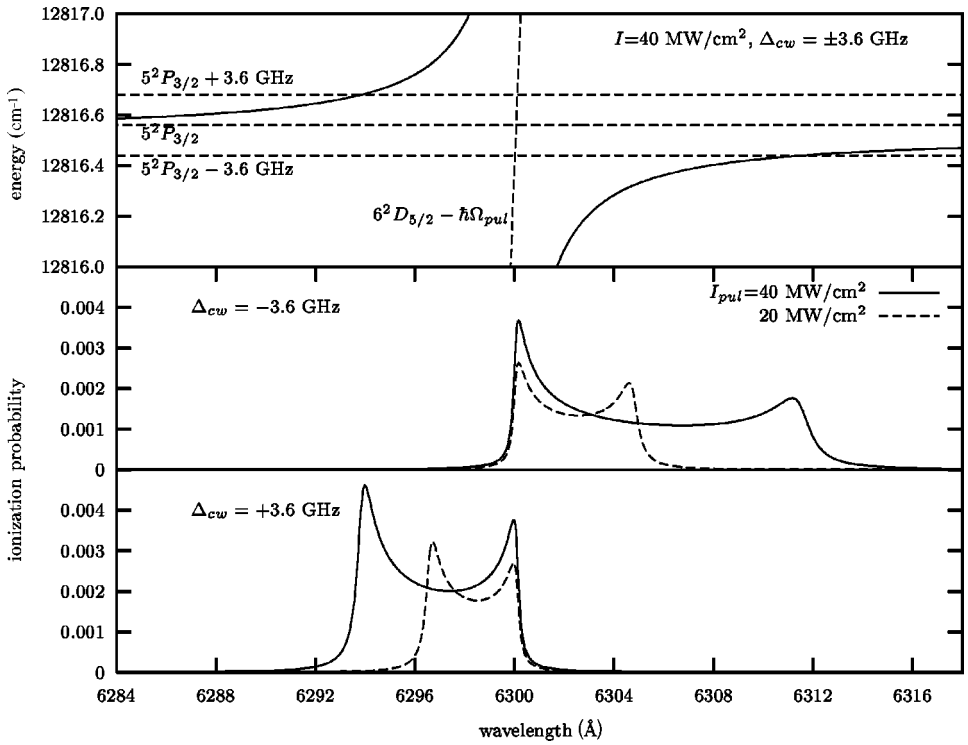

FIG. 4. Line shapes according to a naive Floquet treatment (see Sec. III B). In the upper panel, the dashed lines indicate unperturbed dressed levels, while the full lines are Floquet eigenvalues computed for $I=40$ MW/cm^2. The ionization probability scale is arbitrary.

In principle, Floquet's theory as such can only be applied to cw fields. As one of the two lasers is pulsed, in the following sections we shall adopt an explicit time-dependent approach. However, before going into the details of the spectral simulations, we outline a heuristic description of the three-level system interacting with a weak cw and a strong pulsed radiation, which is useful to understand the numerical results to be presented in the following. Given a very long laser pulse, we can divide it in several time intervals: within each interval, the field amplitude can be considered approximately constant, so that the Floquet treatment is valid. Then, the overall line shape is made of a superposition of peaks, each approximately centered at $\overline{\Delta}_{\rm pul}$ as given by Eq. (4), with I varying from very small (in the pulse tails) to $I_{\rm pul}$ (for $t \simeq t_0$). The shape of a resonance with a given I can be computed exactly within Floquet's theory, and Fig. 4 shows the result of summing many such contributions, with different values of I. The I distribution for most laser pulses would be bell-shaped: in fact, we take it proportional to the square of the pulse envelope function $f(t-t_0)$, Eq. (2). Therefore the lowest and the highest I values have a larger weight than the intermediate ones: this is why the overall line shape is bimodal. One of the peaks, due to the low I contributions, is always close to the ω_2 resonance, but slightly displaced towards blue or red according to the sign of $\Delta_{\rm cw}$. The position of the other peak (high I) is approximated by Eq. (4) with $I=I_{\rm pul}$. In the following, we shall refer to these two features as the ''inner'' and ''outer'' peak, respectively. The asymmetry of the outer peak versus the sign of $\Delta_{\rm cw}$ is quite apparent in the line shapes of Fig. 4 and is due to the $5^2S_{1/2}$-$5^2P_{3/2}$ coupling.

The $5^2P_{3/2}$-$6^2D_{3/2}$ transition is much weaker than the $5^2P_{3/2}$-$6^2D_{5/2}$ one, the ratio of the relevant Clebsch-Gordan coefficients being $1:3\sqrt{6}$. Therefore for the $5^2S_{1/2}$-$5^2P_{3/2}$-$6^2D_{3/2}$ system the A and B coefficients in Eq. (4) are 54 times smaller than in the previous case. No significant shift or doubling of the resonance is expected at the intensities we shall investigate: just a single peak centered at $\Delta_{\rm pul}=2.3$ cm^{-1} (about 0.9 Å in the wavelength scale), which is the $6^2D_{5/2}$-$6^2D_{3/2}$ fine splitting. This peak will lie beside the stronger $5^2P_{3/2}$-$6^2D_{5/2}$ absorption for $\Delta_{\rm cw}>0$, and on top of it for $\Delta_{\rm cw}<0$. This effect contributes to the asymmetry of the line shapes and affects essentially the inner peak with negative $\Delta_{\rm cw}$, as we shall see in the next section.

The approximate treatment just described would be valid for a pulse length τ much longer than the Rabi flopping period of the transitions induced by the cw radiation ($T_{\rm Rabi}=2\pi/\Omega_{\rm Rabi}$). With $I_{\rm cw}=1$ W/cm^2, we have $T_{\rm Rabi}=14.4$ ns at resonance, and $T_{\rm Rabi}=0.278$ ns for a detuning of ± 0.12 cm$^{-1}=\pm 3.6$ GHz. It is clear that the requirement $\tau \gg T_{\rm Rabi}$ is not fulfilled for all conditions, so the results of this section should be just seen as the limiting case for $\tau\rightarrow\infty$ and taken as a qualitative guide to interpret the computed line shapes, which will be presented in the next section.

C. Line-shape simulations

We have computed the populations of the atomic states by direct solution of the time-dependent Schrödinger equation [18]. The coupled differential equations obtained by expansion in eigenstates $|K\rangle$ of the atomic Hamiltonian and of the angular momentum operators J^2 and J_z are

$$i\hbar\frac{dC_K}{dt}=-\sum_{K'} C_{K'}(t)\langle K|\mathbf{d}|K'\rangle\cdot\boldsymbol{\mathcal{E}}(t)e^{i(E_K-E_{K'})t/\hbar}, \quad (5)$$

where C_K is the coefficient of state $|K\rangle$, E_K its energy, and $\mathbf{d}$ is the dipole operator. The numerical integration of these

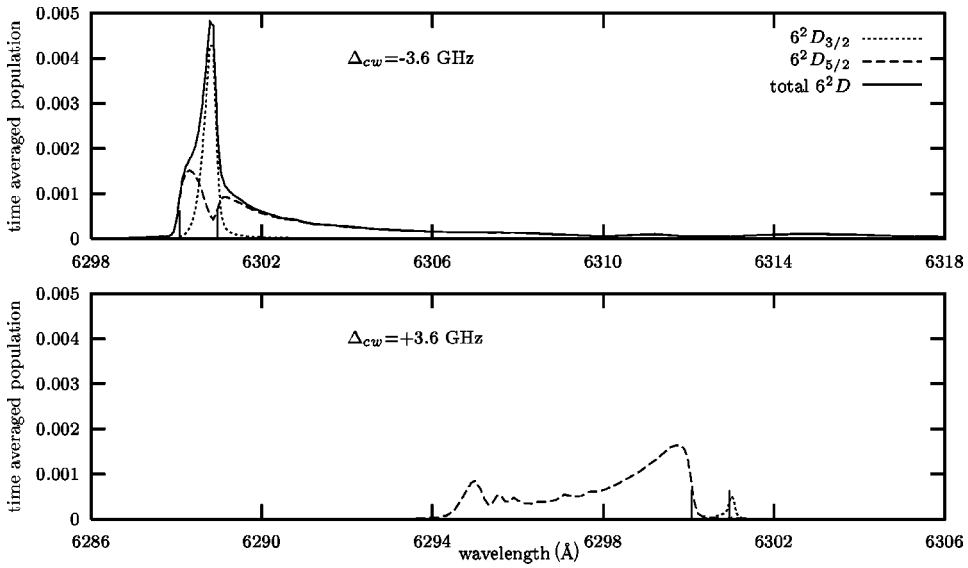

FIG. 5. Line shapes computed as time averaged populations of the 6^2D_J states, without taking into account ionization. The total $6^2D_{3/2}+6^2D_{5/2}$ population (full line) has been omitted in the lower panel because the two components give place to almost completely disjoint line shapes, which coincide with the total in the respective ranges. Vertical bars mark the $5^2P_{3/2}\rightarrow 6^2D_{3/2}$ and $5^2P_{3/2}\rightarrow 6^2D_{5/2}$ transitions, at $\lambda=6300.96$ and 6300.07 Å, respectively.

equations was performed by the sixth order Runge-Kutta-Fehlberg method [19], with a time step of 0.2 fs.

The continuum states of ^2P and ^2F symmetry which describe ionization were introduced in this scheme as rapidly decaying metastable states $|K\rangle$. Energies E_K, lifetimes τ_K, and reduced transition dipoles $\langle 6D|d|K\rangle$ were determined so as to fit the *ab initio* data for the photoionization starting from the $6D$ level, with a Lorentzian form of the oscillator strength:

$$\frac{df}{d\Omega}=\frac{2\pi\hbar^2\langle 6D|d|K\rangle^2}{3}\frac{\tau_K^{-1}}{(\hbar\Omega-E_K+E_{6D})^2+(\hbar/2\tau_K)^2}. \tag{6}$$

The results of the fitting are seen in Fig. 3. The fitting parameters for the ^2P and ^2F states were $E_K=40\,420$ and $36\,950$ cm^{-1}, $\tau_K=0.93$ and 1.17 fs, and $\langle 6D|d|K\rangle=0.278$ and 1.645 a.u., respectively. The finite (indeed very short) lifetime of the ionizing states is introduced in the Schrödinger equation as an imaginary term $-i\hbar/2\tau_K$, added to the energy E_K. In this way the normalization of the time-dependent wave function is not conserved: the missing population, after the end of the laser pulse, corresponds to the ionization probability of a single atom.

In the absence of the pulsed radiation, we only have Rabi oscillations between the $5^2S_{1/2}$ and $5^2P_{3/2}$ levels. When the pulsed light is introduced, the outcome depends on the phase of the Rabi oscillations at the switching on time. Since of course the phase is not controlled in real experiments, we should average over all possible phases. In practice, we found that the same ionization probability is obtained by averaging the results of just two calculations, done with central pulse times t_0 differing by $T_{\mathrm{Rabi}}/2$.

As a link between the simplified theory of the preceding section and the full simulations done with the model just described, we have also computed excitation probabilities to the $6^2D_{3/2}$ and $6^2D_{5/2}$ states, without considering the ionization step. The line shapes, expressed as time-averaged populations of the $6^2D_{3/2}$ and $6^2D_{5/2}$ levels, are shown in Fig. 5. The results of the complete simulations, i.e., the ionization probabilities as functions of the pulsed laser wavelength, are shown in Figs. 6 and 7. In these figures we can single out the results obtained for $I_{\mathrm{pul}}=40$ MW/cm^2 and parallel polarizations of the two lasers, to be compared with those shown in Fig. 5. It can be seen that the assumption made at the beginning of Sec. III A, namely that the ionization rate is proportional to the $6D_J$ populations, is substantially valid, since the line shapes of Fig. 5 are quite similar to those shown in the other figures. Moreover, the results of Fig. 5 allow us to assess the importance of the $5^2S_{1/2}$-$5^2P_{3/2}$-$6^2D_{3/2}$ ionization route, relative to the $5^2S_{1/2}$-$5^2P_{3/2}$-$6^2D_{5/2}$ one. The former is responsible for the small peak at about 6301 Å, which is separate from the main feature of the spectrum for $\Delta_{\mathrm{cw}}>0$. In the negative Δ_{cw} case, the $5^2S_{1/2}$-$5^2P_{3/2}$-$6^2D_{3/2}$ route borrows intensity from the other one, thanks to the population of the common intermediate state $5^2P_{3/2}$, and makes a taller peak on top of the broader $5^2S_{1/2}$-$5^2P_{3/2}$-$6^2D_{5/2}$ line shape: around 6301 Å, the $6^2D_{5/2}$ population is even slightly diminished by competition with the other excitation route. Another way to describe the same phenomenon makes reference to the dynamic Stark shift, mainly caused by the strong $5^2P_{3/2}$-$6^2D_{5/2}$ interaction, which brings into resonance also the $5^2S_{1/2}$-$5^2P_{3/2}$-$6^2D_{3/2}$ pathway. Overall, ionization alters only slightly the relative importance of the distinct features which can be seen also in Fig. 5: inner and outer peaks, and the $6^2D_{3/2}$ resonance.

In Fig. 6 we show the dependence of the line shape on the peak intensity of the pulsed laser, I_{pul}. The main effect of increasing I_{pul}, as expected, is to shift the outer peak, which broadens to form a long tail in the case of negative Δ_{cw}, while it takes an increasing importance for positive Δ_{cw}. Also the inner peak slightly shifts further off resonance by increasing I_{pul}: as a consequence, its position with respect to the $6^2D_{3/2}$ resonance changes gradually, and so does the $\Delta_{\mathrm{cw}}<0$ line shape, which is a superposition of these two features.

In Fig. 7 we show results obtained with perpendicular polarizations of the two lasers ($\boldsymbol{\mathcal{E}}_{\mathrm{cw}}^{(0)}\perp\boldsymbol{\mathcal{E}}_{\mathrm{pul}}^{(0)}$). Because of the

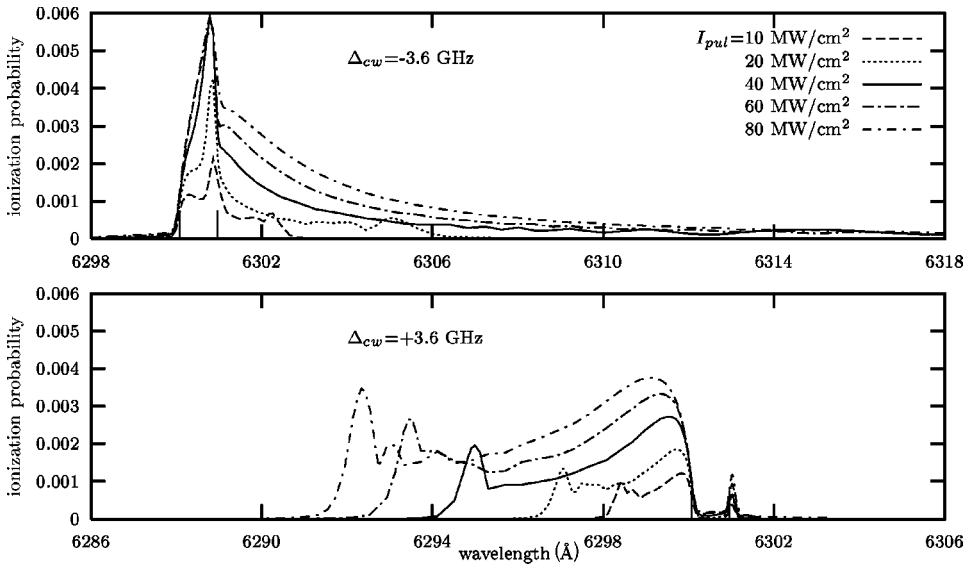

FIG. 6. Line shapes, computed as single atom ionization probabilities, with different peak intensities $I_{\rm pul}$. Vertical bars mark the $5^2P_{3/2}\rightarrow 6^2D_{3/2}$ and $5^2P_{3/2}\rightarrow 6^2D_{5/2}$ transitions, at $\lambda = 6300.96$ and 6300.07 Å, respectively.

different Clebsch-Gordan coefficients, the $5^2S_{1/2}$-$5^2P_{3/2}$-$6^2D_{3/2}$ route is here much more important than with parallel polarizations.

IV. COMPARISON OF SIMULATIONS AND EXPERIMENTS

It is quite evident that the simulated line shapes exhibit many common features with the experimental ones. However, there are also some important differences. In both cases we find that the stronger ionization is blue detuned with respect to the $5^2P_{3/2}$-$6^2D_{5/2}$ transition if $\Delta_{\rm cw}>0$ and red detuned if $\Delta_{\rm cw}<0$. The broad peak close to 6300 Å is taller for negative than for positive $\Delta_{\rm cw}$: this is due to the superposition of the $5^2P_{3/2}$-$6^2D_{3/2}$ and $5^2P_{3/2}$-$6^2D_{5/2}$ transitions. A smaller peak, due to the $5^2P_{3/2}$-$6^2D_{3/2}$ resonance, is found at about 6301 Å when $\Delta_{\rm cw}>0$.

The most striking difference between the simulated and the experimental spectra is the presence of an ''outer'' peak only in the former, while the measured line shapes vanish smoothly for large detunings $\Delta_{\rm pul}$. This is mainly due to fluctuations and inhomogeneity of the pulsed laser intensity. We evaluate that the peak intensity of each pulse in our apparatus fluctuates around a central value with a Gaussian distribution and a standard deviation σ of about 30%. Moreover, the laser beam is not homogeneous, and has approximately the same diameter as the MOT. We shall assume that the photon flux decreases as a Gaussian function exp $(-R^2/R_0^2)$ of the distance from the beam axis, R. The observed line shape $\overline{S}$ will then be the result of two averaging operations, over a large number of pulses and over the beam cross section. Let us call $S(I_{\rm pul},\Delta_{\rm pul})$ the computed line shape for a given $I_{\rm pul}$. We have:

$$\overline{S}(\overline{I_{\rm pul}},\Delta_{\rm pul})=\frac{\sqrt{2\pi}}{\sigma}\int_0^\infty dI_{\rm pul}e^{-(I_{\rm pul}-\overline{I_{\rm pul}})/2\sigma^2}\times\int_0^{R_{\rm max}}RdRS(I_{\rm pul}e^{-R^2/R_0^2},\Delta_{\rm pul}),\qquad(7)$$

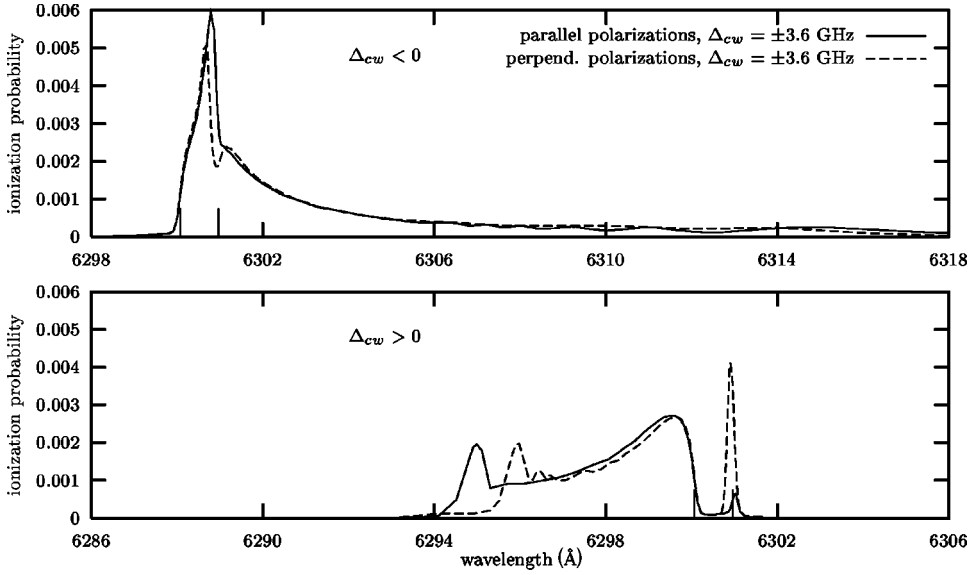

FIG. 7. Comparison of line shapes (single atom ionization probabilities) with perpendicular versus parallel polarizations of the cw and pulsed lasers.

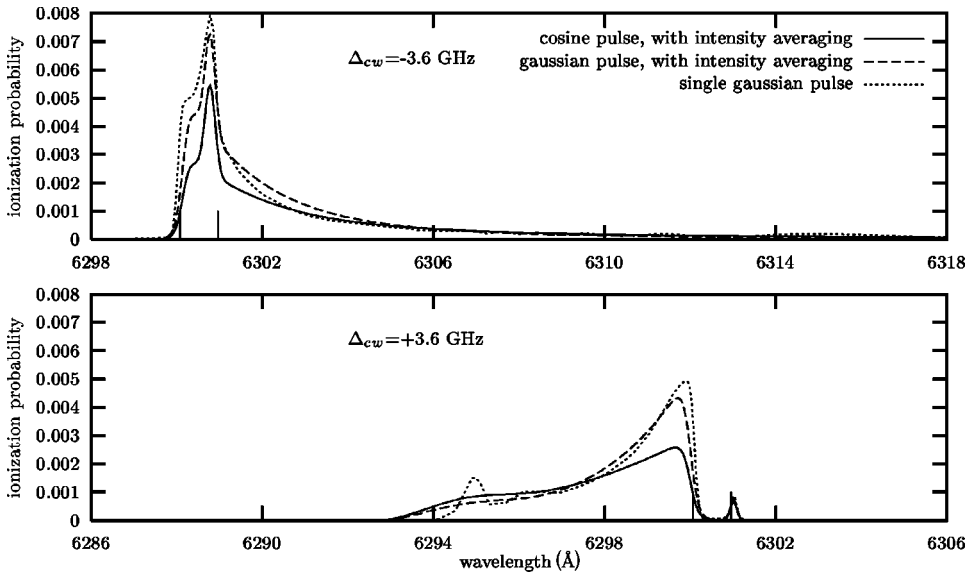

FIG. 8. Full line: line shape (single atom ionization probability) obtained by averaging over the pulsed laser intensity, with central value $\overline{I_{\rm pul}}=40$ MW/cm^2. Dashed line: same with a Gaussian pulse. Dotted line: single Gaussian pulse (without intensity averaging), with $I_{\rm pul}=40$ MW/cm^2. The ionization probabilities obtained with Gaussian pulses have been rescaled by a factor $1/\sqrt{(\pi)}$, which accounts for the ratio of the total energies of pulses with different envelopes.

where $\sigma=0.30$. The cutoff radius $R_{\rm max}$ takes into account in the simplest way the MOT boundaries, as if the atom density would drop to zero for $R>R_{\rm max}$. The value of the integral only depends on the ratio $R_{\rm max}/R_0$, which we shall assume equal to 1. We fitted the line shapes of Fig. 6, together with many more results computed to this purpose, with an analytic function of $I_{\rm pul}$ and $\Delta_{\rm pul}$, which was used to calculate $\overline{S}$ by numerical quadrature. The resulting line shapes are shown in Fig. 8. The ''outer'' peak has almost completely disappeared because its position depends on the intensity, and in the averaging operation it is smeared out over a wide range of wavelengths. After this operation, only a slight bump remains in the case of positive $\Delta_{\rm cw}$. Hence the basic asymmetry versus the sign of $\Delta_{\rm cw}$, affecting the outer peak in Figs. 4–6, eventually manifests itself as a difference in the extension of the tails in the line shapes.

Even with intensity averaging, the agreement between computed and observed line shapes is not perfect. For positive $\Delta_{\rm cw}$, the experimental spectrum shows a sharper peak with a less substantial queue on the blue side. A possible source of discrepancy is the pulse shape, given by Eqs. (1) and (2). In Fig. 6 we also show results obtained with a Gaussian envelope:

$$f(t-t_0)=e^{-(t-t_0)^2/\tau^2}. \tag{8}$$

The intensity averaging of the line shape in this case was not done directly because we did not compute line shapes for variable $I_{\rm pul}$ with a Gaussian pulse. Therefore we resorted to a mapping of the line shape obtained with pulses of finite length into that of the Gaussian pulse, by means of a multiplicative function of $I_{\rm pul}$ and $\Delta_{\rm pul}$, in order to have the necessary data for the quadrature (7). The Gaussian pulse yields line shapes closer to the experimental ones, in that the inner peak, both for $\Delta_{\rm cw}>0$ and for $\Delta_{\rm cw}<0$, is sharper and taller. Moreover, the outer peak is comparatively less important, and so is the bump in the queue of the averaged line shape. All this is due to the low intensities, which contribute to the inner peak, having a larger weight in the Gaussian envelope with respect to that of Eq. (2).

Lastly, we have tested the effect of a finite coherence time of the pulsed laser. The linewidth of 10 GHz, for a perfectly coherent pulse, would correspond to a length shorter than 0.1 ns, depending on the exact shape. In order to simulate a 3 ns pulse with a coherence time of the order of 0.1 ns, we have used a sequence of short pulses, each one with the envelope $\cos[\pi(t-t_k)/2\tau']$ and $\tau'=0.1$ ns. The delay between two successive pulses is $t_{k+1}-t_k=\tau'$, so they partially overlap. The carrier wave for the kth pulse is $\cos(\Omega_{\rm pul}t+\phi_k)$ and the phases ϕ_k are random numbers. In this way we have phase conservation for $\Delta t\ll 0.1$ ns, and uncorrelated phases for $\Delta t\gg 0.1$ ns. The amplitude of the electric field is further modulated by the same function as in Eq. (2), with $\tau=3$ ns. Of course the results depend on the random phases ϕ_k: Fig. 9 shows the average line shapes obtained with four such pulses (for a few wavelengths, we ran 20 calculations in order to have better statistics). Of course, no convolution has been applied in this case, since the real bandwidth of the pulsed laser has been explicitly taken into account. The signal-to-noise ratio is smaller than in the measured spectra, which are the result of averaging over 30 pulses. However, it is apparent that the phase fluctuation affects the line shapes and improves the agreement with the experiment. With both positive and negative $\Delta_{\rm cw}$, the inner peak is taller and the increase of the intensity around $\lambda=6300$ Å is steeper than in the case of a perfectly coherent pulse. The outer peak, on the contrary, is less well-defined: the combined effects of finite coherence time and intensity averaging would probably wash it out even for positive $\Delta_{\rm cw}$. In general, phase fluctuations influence all the features that are sensitive to early times or small intensities of the pulsed laser application; they flatten the contributions deriving from the narrower bandwidth lines, and in particular the importance of the $6^2D_{3/2}$ peak with positive $\Delta_{\rm cw}$, for both parallel and perpendicular polarizations. This effect was introduced in the other simulations by a Gaussian convolution of the line shape and the obtained

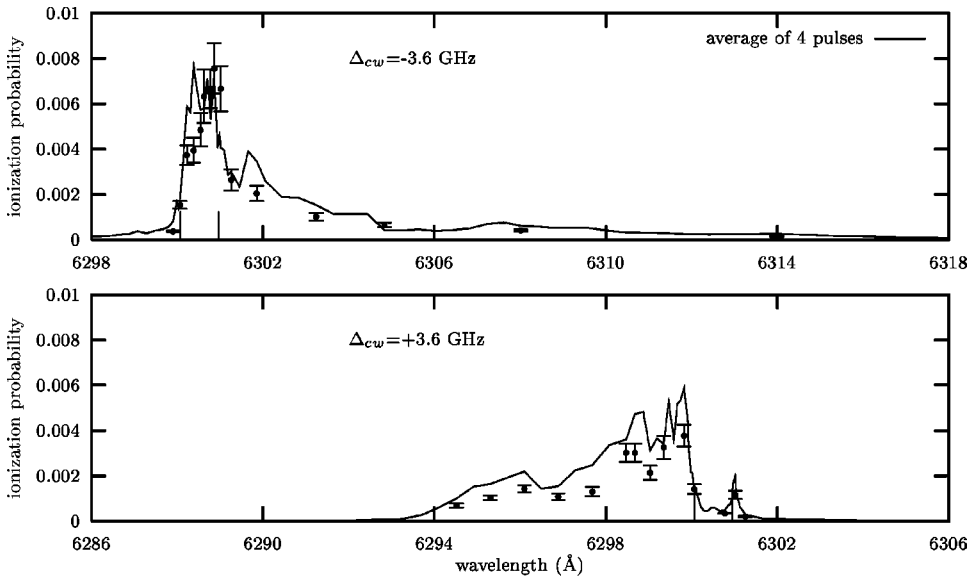

FIG. 9. Line shapes (single atom ionization probabilities) obtained with phase fluctuations for the pulsed laser. Full line: average of four pulses with different random phases. Full circles with error bars corresponding to one standard deviation represent 20 pulse averages, calculated only for a few wavelengths.

results confirm the substantial correctness of the procedure in this case.

We can finally compare the absolute magnitude of the experimental signals and the theoretical ionization probability. The ion peaks of Fig. 1 for parallel polarizations, taken with a cw laser intensity of 5 W/cm^2 and a pulsed laser intensity of 40 MW/cm^2, are about 6×10^4 and 2×10^4 ions for negative and positive detuning, respectively. Since the trapped atom number is 10^7 and the estimated total detection efficiency is 0.2, the corresponding ionization probabilities are about 3% and 1%. We stress that the rather large uncertainties which affect some of the experimental parameters, such as the atom density and the cw laser fluence, do not affect the line shapes: on the other hand, only the order of magnitude of the atomic ionization probabilities can be estimated. With this in mind, we can compare them with the theoretical probabilities obtained in the same conditions: the average of 20 pulses with phase fluctuations (dots in Fig. 8) yields $3.8\pm0.6\%$ and $1.9\pm0.3\%$, for negative and positive detuning, respectively. The ratio of the two peaks is therefore 2.0 ± 0.4, versus an experimental value of 3.

V. CONCLUSIONS

We have observed strongly asymmetric line shapes in a two-color, three-photon ionization process, involving excitation to the 6^2D_J levels by quasi-resonant interactions with cw and pulsed laser radiations, and the subsequent transition to the ^2P or ^2F electronic continua. We have explained the origin of the observed line shapes by a time-dependent simulation of the radiation-atom interactions, with proper consideration of the ionization process, based on *ab initio* calculations of the bound-free transition dipoles.

The asymmetric line shapes, i.e., the fact that the ionization is intense only when both the cw and the pulsed laser are either red or blue detuned, are a manifestation of the Autler-Townes effect (the detuning of the cw laser is always referred to the $5^2S_{1/2}$-$5^2P_{3/2}$ transition and that of the pulsed laser to the $5^2P_{3/2}$-$6^2D_{5/2}$ one). Because the pulsed laser intensity varies in time through the whole interval between zero and the peak intensity I_{pul}, one obtains an extended line shape rather than a narrow peak. Any pulse of coherent light with a bell-shaped temporal dependence of intensity would produce a bimodal line shape: one of the maxima would be close to resonance, and the other one blue or red shifted by an amount depending on I_{pul} (Fig. 6). This fact is brought out both by simulations with two different pulse shapes and by a heuristic model based on a three-state Floquet treatment, useful for a qualitative understanding of the phenomenon. The experimental line shapes, on the other hand, only exhibit the near resonance maximum, with long tails which smoothly decay. The tail is longer for negative than for positive detuning because of the $5^2S_{1/2}$-$5^2P_{3/2}$ interaction, which induces an upward dynamic shift of the $5^2P_{3/2}$ level. In fact, we have shown by additional sets of simulations that two characteristics of the laser radiation are important to obtain an agreement between theoretical and measured line shapes: one is the dispersion of pulse intensities (Fig. 8), and the other one is the finite coherence time of the pulsed laser (Fig. 9).

Another kind of asymmetry, namely that the red detunings produce a stronger signal than the blue ones, is due to the existence of two excitation routes, $5^2S_{1/2}$-$5^2P_{3/2}$-$6^2D_{5/2}$ and $5^2S_{1/2}$-$5^2P_{3/2}$-$6^2D_{3/2}$. The former pathway is responsible for the main features of the line shapes, as outlined above. The other pathway, involving the weaker $5^2P_{3/2}$-$6^2D_{3/2}$ transition, produces a small isolated peak with blue detuning, while it is superimposed to the $6^2D_{5/2}$ line shape with red detuning: as a consequence, in the latter case the $6^2D_{3/2}$ contribution is enhanced by the dynamic Stark shift of the $5^2P_{3/2}$ level caused by the strong $5^2P_{3/2}$-$6^2D_{3/2}$ interaction. The finite coherence time of the pulsed laser was important also in determining the relative effectiveness of the two excitation routes.

Overall, we have shown that a semiquantitative agreement between simulated and measured line shapes can be reached by taking into account some relevant features of the laser radiation: namely, pulse shape, pulse intensity distribution

and finite coherence time. We feel this strategy, together with the simplified heuristic model we introduced, is apt to shed light on all the important physical aspects of this multiphoton ionization process.

ACKNOWLEDGMENTS

We would like to thank E. Arimondo, N. Beverini, and R. Pratesi for lending us part of the experimental equipment.

[1] J. Szudy and W. E. Baylis, Phys. Rep. **266**, 127 (1996).
[2] C. Gabbanini, A. Fioretti, A. Lucchesini, S. Gozzini, and M. Mazzoni, Phys. Rev. Lett. **84**, 2814 (2000).
[3] B. C. Duncan, V. Sanchez-Villicana, P. L. Gould, and H. R. Sadeghpour, Phys. Rev. A **63**, 043411 (2000).
[4] G. S. Agarwal, Phys. Rev. Lett. **37**, 1383 (1976).
[5] J. K. Eberly, Phys. Rev. Lett. **37**, 1387 (1976).
[6] S. N. Dixit, P. Zoller, and P. Lambropoulos, Phys. Rev. A **21**, 1289 (1980).
[7] M. Kus and M. Lewenstein, J. Phys. B **14**, 4933 (1981).
[8] Th. Hslwanter, H. Ritsch, J. Cooper, and P. Zoller, Phys. Rev. A **38**, 5652 (1988).
[9] A. T. Georges and P. Lambropoulos, Phys. Rev. A **18**, 587 (1978).
[10] P. B. Hogan, S. J. Smith, A. T. Georges, and P. Lambropoulos, Phys. Rev. Lett. **41**, 229 (1978).
[11] A. Fioretti, C. Gabbanini, M. Persico, I. Cacelli, and M. Mazzoni, in *Spectral Line Shapes*, AIP Conf. Proc. No. 559, edited by J. Seidel (AIP, Melville, NY, 2001), pp. 293–295.
[12] I. Cacelli, V. Carravetta, and R. Moccia, Chem. Phys. **90**, 313 (1984).
[13] I. N. Shabanova and A. N. Khlyustalov, Opt. Spectrosc. **56**, 128 (1984).
[14] R. F. Gutterres, C. Amiot, A. Fioretti, C. Gabbanini, M. Mazzoni, and O. Dulieu, Phys. Rev. A. (to be published).
[15] M. Marinescu and A. Dalgarno, Phys. Rev. A **52**, 311 (1995).
[16] M. Marinescu, H. R. Sadeghpour, and A. Dalgarno, Phys. Rev. A **49**, 5103 (1994).
[17] S. H. Autler and C. H. Townes, Phys. Rev. **100**, 703 (1955).
[18] M. Malvaldi, M. Persico, and P. Van Leuven, J. Chem. Phys. **111**, 9560 (1999).
[19] G. Jordan-Engeln and F. Reutter, *Formelsammlung zur Numerischen Mathematik* (Bibliographic Institute Mannheim, Wien, 1981).